GEOPHYSICS, VOL. 71, NO. 6 (NOVEMBER-DECEMBER 2006); P. B201–B209, 15 FIGS.
10.1190/1.2348780

Exploration for unconformity-type uranium deposits with audiomagnetotelluric data: A case study from the McArthur River mine, Saskatchewan, Canada

Volkan Tuncer[1], Martyn J. Unsworth[1], Weerachai Siripunvaraporn[2], and James A. Craven[3]

ABSTRACT

Unconformity-type deposits supply a significant amount of the world's uranium and consist of uranium that is generally codeposited with graphite in a fault zone. The low resistivity of the graphite produces a significant contrast in electrical resistivity, which can be located with electromagnetic (EM) methods. The Athabasca Basin in Western Canada hosts significant uranium deposits, and exploration in deeper parts of the basin has required the application of new EM methods. This paper presents an evaluation of the audiomagnetotelluric (AMT) exploration method at the McArthur River mine in the Athabasca Basin. AMT data were collected at 132 stations on a grid, and two-dimensional (2D) and three-dimensional (3D) inversions were used to generate resistivity models. These models showed two major results: (1) a significant conductor coincident with a major basement fault (P2) and the uranium deposits (this conductor begins at the unconformity at a depth of 550 m and extends to a depth of at least three km) and (2) a resistive halo which might be caused by the silicification associated with mineralization. However, synthetic inversions showed that this halo could be an artifact of smoothing function in the inversion scheme. The 2D inversions were validated by synthetic inversions, comparison with the 3D inversion models, and correlation with well-log information. 3D AMT forward modeling showed that strong 3D effects are not present in the AMT impedance data. Induction vectors showed more evidence of complexity, but the inclusion of these data in the inversion improved subsurface resolution.

INTRODUCTION

Unconformity-type deposits are a major source of uranium. The Athabasca Basin, located in northwest Saskatchewan and northeast Alberta, produces one-third of the Western world's uranium (Jefferson et al., 2003). As exploration has proceeded, many of the shallowest deposits have been mined out, and exploration has moved into deeper parts of the basin. This is challenging existing exploration methods, and government and industrial partners initiated the EXTECH-IV (EXploration science and TECHnology initiative) project to develop new techniques for locating unconformity-type uranium deposits. The EXTECH-IV project has included a range of geophysical and geological studies (Jefferson et al., 2003). Most of the geophysical studies took place at the McArthur River mine, which hosts the largest known high-grade uranium deposit in the world.

Electrical and electromagnetic (EM) methods are widely used in mineral exploration and have played an important role in uranium exploration in the Athabasca Basin (McMullan et al., 1987; Crone, 1991). The uranium deposits are found where basement faults intersect the unconformity (Figure 1). Because graphite is commonly found in the faults, the resulting low electrical resistivity often allows detection with EM methods. However, not all unconformity-type uranium deposits occur above or within graphitic faults. As part of the EXTECH-IV project, alternative EM methods were evaluated to determine if they could map basement conductors at depth in the Athabasca Basin. One such method is the audiomagnetotelluric (AMT) method, which uses natural EM signals to image the upper 1–2 km of the subsurface. In contrast to loop-loop EM methods and the controlled-source audiomagnetotelluric (CSAMT) method, AMT is logistically simple because no transmitter is required. In this paper, a pilot AMT survey over a known uranium deposit is described.

Manuscript received by the Editor May 4, 2005; revised manuscript received March 7, 2006; published online October 3, 2006.
[1]University of Alberta, Department of Physics, Edmonton, Alberta, Canada. E-mail: vtuncer@phys.ualberta.ca; unsworth@phys.ualberta.ca.
[2]Mahidol University, Department of Physics, Faculty of Science, Bangkok, Thailand. E-mail: scwsp@mahidol.ac.th.
[3]Geological Survey of Canada, 601 Booth Street, Ottawa, Ontario, Canada. E-mail craven@NRCan.gc.ca.

GEOLOGIC SETTING AND MINERALIZATION

At the McArthur River mine, the near-surface structure is characterized by overburden that is up to 100 m thick. The underlying Athabasca Group rocks (Figure 1) are sandstones and conglomerates of late paleo- to Meso-Proterozoic age (Ruzicka, 1996). Beneath the unconformity, the crystalline (gneissic) basement comprises the 2.5–2.6-Ga (billion years ago) Wollaston Group (McMullan et al., 1987). Uranium deposits in the Athabasca Basin are structurally controlled by the Paleo-Proterozoic (sub-Athabasca) unconformity and faults that exhibit a northeastern or eastern strike (Ruzicka, 1996). The uranium orebodies range in shape from massive subhorizontal lenses at the unconformity to veins and veinlets in the fault zones (Ruzicka, 1996). The deposits formed where oxidizing basinal fluids carried uranium from the sandstone and reducing fluids carried other minerals (such as silica) from the basement rocks to the unconformity through the fault (Figure 1). This deposited uranium at the top of the fault near the unconformity; silicification occurs above the unconformity because of the fluid flow. Prior to uranium ore deposition, intense silicification developed where ascending fluids flooded the sandstone with quartz. Significant silicification surrounds the ore deposit at the McArthur River, although most other Athabasca Basin deposits are surrounded by extensive zones of quartz dissolution (Ruzicka, 1996). In addition, a thin alteration halo of quartz dissolution and illite clay alteration was formed around the uranium deposit (Ruzicka, 1996). Mwenifumbo et al. (2004) suggested that at McArthur River, silicification is localized between the unconformity and a depth of 375 m. Limited alteration has occurred in the basement gneisses (Ruzicka, 1996), and hydrothermal clay alteration is spatially limited at McArthur River (Mwenifumbo et al., 2004).

Polymetallic deposits (U-Ni-Co-As) occur more often within the unconformity, although monometallic deposits occur either below or rarely above the unconformity. The monometallic-type McArthur River P2 North deposit is the only known exception from this rule (Ruzicka, 1996). Pods of the McArthur River P2 North deposit extend 60 m downdip along the P2 fault zone from immediately beneath the unconformity in the footwall and just above the P2 reverse fault in the nose of the uplifted hanging wall basement wedge. This southeast-dipping reverse fault offsets the basement by 60–80 m. The approximate size of the orebody is 100 m long, 10 m wide, and 60 m high, and is located between depths of 500 and 600 m (Ruzicka, 1996).

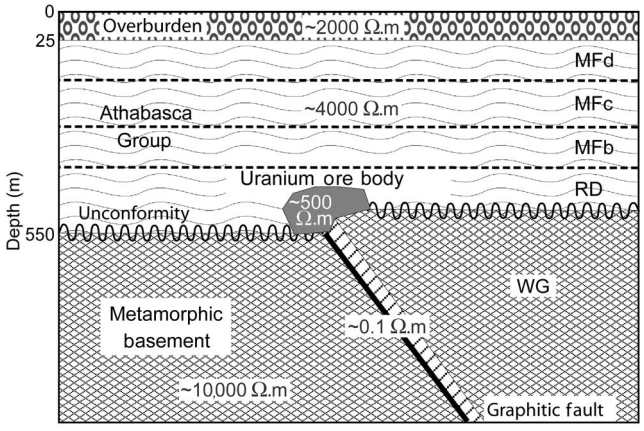

Figure 1. Generic model of an unconformity-type uranium deposit in the Athabasca Basin (after McMullan et al., 1987; Mwenifumbo et al., 2004). The Athabasca Group consists of four major units from bottom to top. The Read Formation (RD, formerly MFa) comprises discontinuous basal conglomerate, intercalated coarse sandstone, conglomerate and red mudstone. The Manitou Falls Formation comprises MFb: interbedded conglomerate and pebbly sandstone; MFc: granule sandstone; and MFd: medium-fine sandstone with mudstone intraclasts. WG is the Wollaston Group.

PREVIOUS GEOPHYSICAL STUDIES

A significant amount of geophysical data has been acquired at the McArthur River deposit, both before and during the EXTECH-IV project. Gravity studies were used to map the depth of the unconformity and to locate zones of alteration (Wood and Thomas, 2002). However, nonuniqueness restricts the ability of gravity data to distinguish between silicified and desilicified zones that might be associated with underlying ore deposits. Seismic reflection data were able to image the unconformity and faults that offset it but did not detect the uranium orebody or graphite directly (Hajnal et al., 2002; White et al., 2002; White et al., 2003). The faults that underlie the uranium deposits are often graphitic. Electrical and EM methods have been used to locate them in the Athabasca Basin. In shallow parts of the basin, basement conductors have been located with direct current (dc) resistivity, transient electromagnetic methods, horizontal-loop EM method (HLEM), and very-low-frequency (VLF) data (Craven et al., 2003). These methods are convenient for shallow exploration but less effective where the target depth exceeds 500 m.

To explore deeper parts of the Athabasca Basin, other EM methods must be used. The pulse EM method (DEEPEM) was used over the Cigar Lake deposit and defined a conductor at a depth of 450 m, but exploration was complicated by the low-resistivity regolith (Crone, 1991). Controlled-source EM exploration at greater depth requires larger loops to be used and thus increases the logistical effort and cost. As exploration expands into the deeper part of the Athabasca Basin, alternative EM methods are needed for effective and economical exploration. The audiomagnetotelluric (AMT) method uses natural EM signals to image near-surface structures. With improved magnetic sensors, it is no longer necessary to use a controlled source, and this has reduced the cost and increased the use of this technique in recent years. Recent applications of AMT in mineral exploration include studies by Livelybrooks et al. (1996), Chouteau et al. (1997), and Jones and Garcia (2003). The EXTECH-IV study described in this paper evaluated the role that AMT could play in uranium exploration in the Athabasca Basin. It was anticipated that AMT could locate basement conductors and determine their depth.

AMT DATA ACQUISITON

AMT data were recorded in 2002 by Geosystem SRL at 132 stations on 11 profiles that crossed the P2 fault (Figure 2). Data collection used Metronix AMT systems, and the magnetic fields were measured with BF-6 and BF-10 induction coils produced by Electro-Magnetic Instruments. The distance between profiles was approximately 800 m, and the station spacing was approximately 300 m. Electric-field dipoles were 50 m in length, and time series were recorded with sampling rates of 40,960, 4096, and 256 Hz. Usable AMT data were obtained over the frequency range 10,200–3 Hz. Coherent time-series segments from each sampling rate were select-

ed automatically for robust analysis to reduce the effects of bias because of noise. An iterative reweighting scheme was used to provide a robust estimate of the apparent resistivities and phases (Larsen et al., 1996).

AMT DATA ANALYSIS

The dimensionality of the AMT data was investigated using tensor decomposition (McNeice and Jones, 2001). In the frequency range of 1000–1 Hz, the geoelectric strike direction is well defined as 45° and parallel to the P2 fault direction (Figure 3). Figure 3 shows the spatial distribution of the rms misfit obtained by the decomposition, and the relatively low values (less than one) suggest that a 2D interpretation was valid. All data then were rotated to a coordinate system with the x-axis in the N45°E direction. Apparent resistivities can be computed from the along-strike electric currents (TE mode) and also from the across-strike electric currents (TM mode). Over a 2D earth, these two modes give different apparent resistivity values and are sensitive to different aspects of the subsurface structure. The TE mode is the most sensitive to along-strike conductors, whereas the TM mode is the most sensitive to resistors and shallow structure (Berdichevsky et al., 1998). AMT data for these two modes are illustrated in pseudosections for line 224 in Figure 4, which shows limited site-to-site variation in apparent resistivity in TE mode because the electric field is parallel to the geoelectric strike. The TM-mode pseudosection shows more site-to-site variation because near-surface bodies strongly affect the apparent resistivity. In the TE-mode pseudosection, the location of the conductor is indicated by generally lower apparent resistivities in the center of the profile. Sample data curves of apparent resistivity and phase from different locations are shown in Figure 5. Note that the TM-mode data are less sensitive to the presence of the basement conductors than the TE-mode data. The TE-mode electric currents generate a vertical magnetic field (H_z), that is related to the horizontal magnetic fields by

$$H_z = T_{zx}H_x + T_{zy}H_y, \quad (1)$$

where T_{zx} and T_{zy} are components of the magnetic field transfer function (tipper). This real transfer function changes sign above a conductor, as observed in Figure 4, with positive values on the left of the conductor and negative signs on the right. This sign reversal at 1.5 km indicates the horizontal location of the conductor. These transfer functions can also be displayed as induction vectors at a given frequency. In the convention of Parkinson (1959), the real part of the induction arrow points toward a conductor. Figure 6 shows the real induction vectors at a frequency of 100 Hz, which sample the subsurface to a depth of approximately 2 km. The direction of the vectors on most profiles shows a reversal, marking the location of a basement conductor. Induction vectors parallel to the profile are an indication of a 2D resistivity structure and are observed on lines 224–248. The situation is more complex to the north, and the induction vectors are at a significant angle to the strike direction. Note that induction vectors show more evidence of 3D behavior than the tensor decomposition. This can be explained because AMT impedances are primarily sensitive to structure below the station, whereas vertical magnetic fields are most sensitive to structures located to one side.

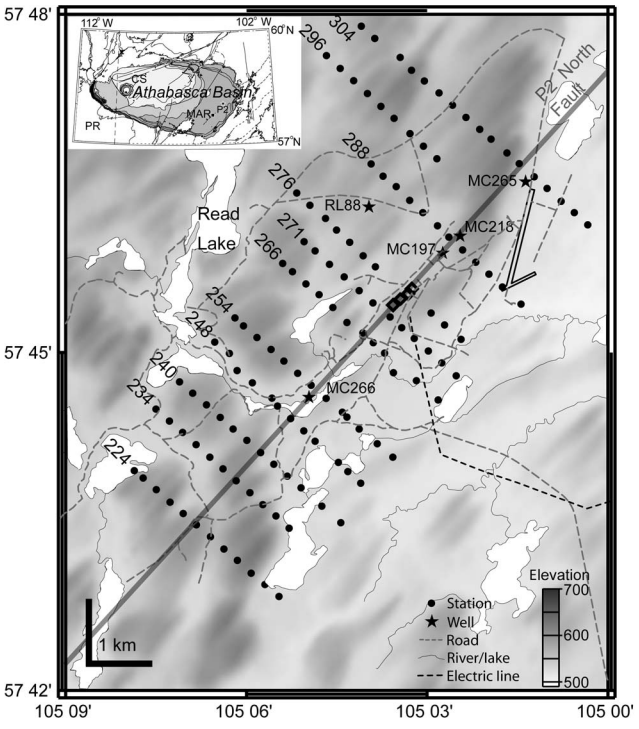

Figure 2. AMT station locations used in the McArthur River AMT survey. Black diamonds on the P2 North Faultline between lines 271 and 276 show the uranium ore pods. (MAR: McArthur River CS: Carswell structure; PR: Phanerozoic rocks, P2: P2 North fault).

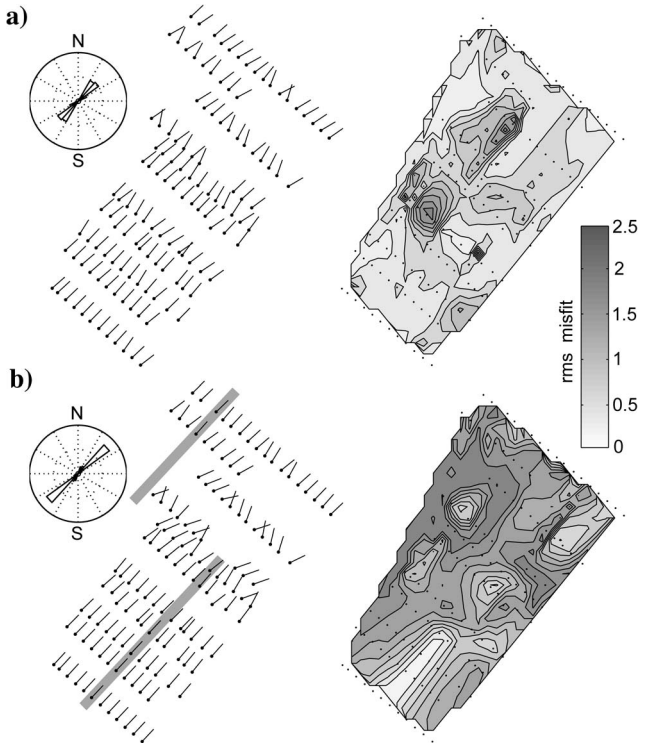

Figure 3. Results of tensor decomposition for real data and synthetic 3D model over frequency range 1000–1 Hz. (a) Shows best-fitting strike direction in map format and the misfit obtained by the tensor decomposition. Low misfit values indicate the 2D assumption is well satisfied. (b) Same quantities for synthetic data generated for a 3D resistivity model. Gray rectangular bars show the locations of conductors in the 3D synthetic models.

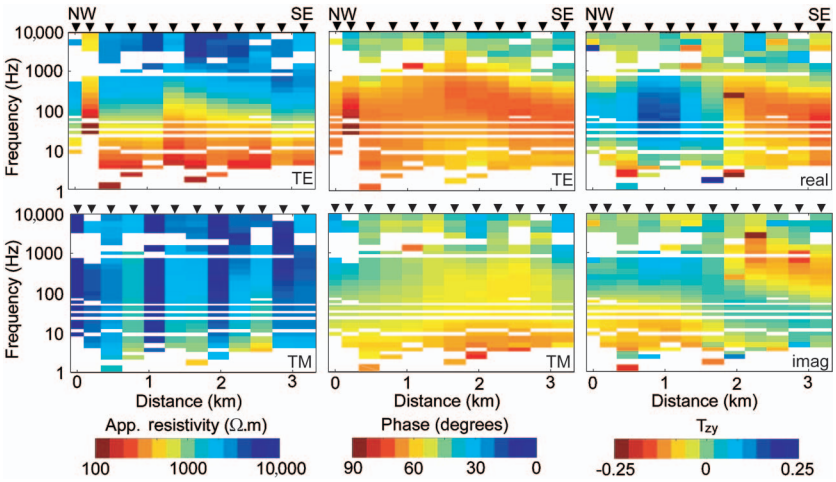

Figure 4. Pseudosections for TE, TM, and magnetic field transfer function data from line 224.

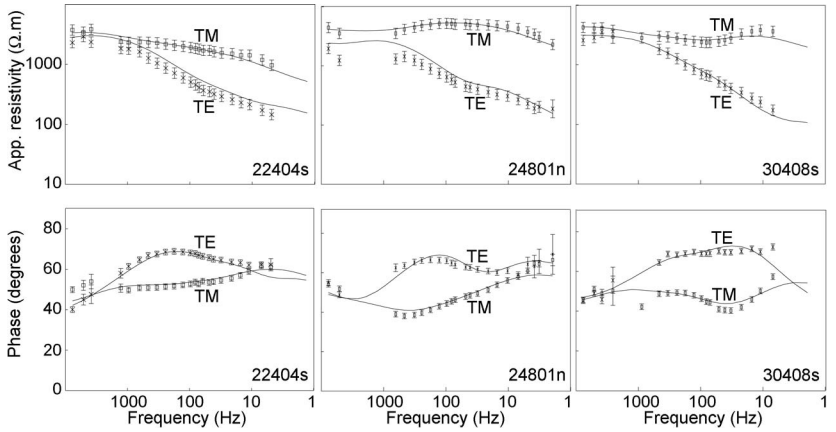

Figure 5. Sample data curves of TE and TM-mode for stations on lines 224, 248, and 304. Continuous lines show the response of the inversion models in Figure 9.

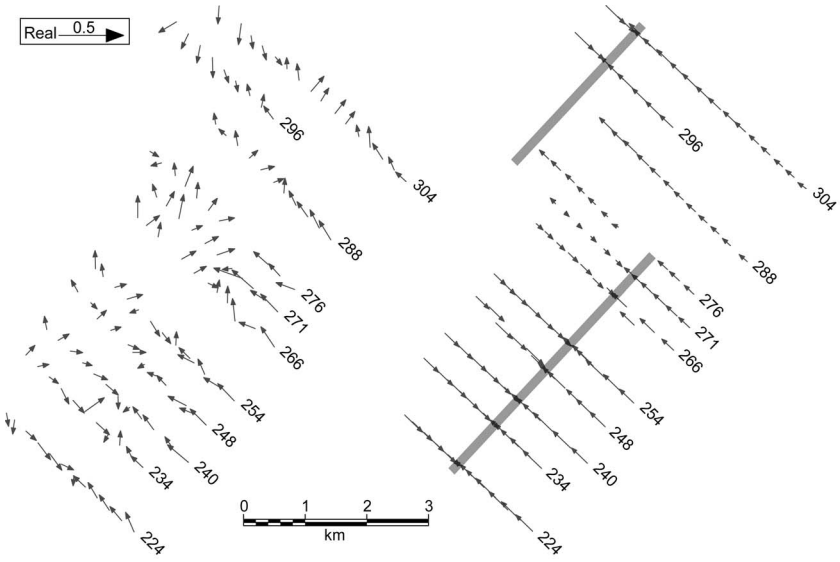

Figure 6. (a) Induction vectors at 100 Hz frequency. Note the real induction vectors point at a conductor. (b) Synthetic induction vectors for a simple 3D model. Gray-shaded rectangular bars show the locations of basement conductors.

INVERSION OF AMT DATA

Two-dimensional inversion

The dimensionality analysis and the similarity of the pseudosections for adjacent profiles suggest that a 2D analysis is valid for these AMT data. For each profile, AMT data were inverted using the nonlinear conjugate gradients (NLCG) algorithm of Rodi and Mackie (2001). This inversion seeks a resistivity model that fits the observed AMT data and which also satisfies a specified regularization function. This generally requires a spatially smooth model but can also include other requirements. AMT data for each profile were inverted with the NLCG6 algorithm. Separate inversions of the TE mode, TM mode, and T_{zy} were used to check the internal consistency of the AMT data (Figure 7). The TE mode is most sensitive to along-strike conductors and clearly images a conductor in the center of profile 224, although the TM mode does not image the conductor at all. The T_{zy} data locate the horizontal position of the conductor but do not determine its depth. To obtain a reliable image of subsurface resistivity, joint inversion of all data is required and gives a sharper image of the basement conductor (Figure 7). The fit of the model response to the measured data is shown at selected stations in Figure 5, and the fit at other stations is of similar quality. Static shifts encountered in the data were small, and it was not necessary to correct for them explicitly. The error floors used in these inversions for apparent resistivity, phase, and tipper are 20%, 5%, and 0.025, respectively. Lower error floors were also applied to the apparent resistivity, but models were rougher with low error floors (e.g., 10%). Simultaneous inversion of all data gave very similar models to those obtained by a sequential approach (TE or TE-TM first, then TE-TM-T_{zy}). Resistivity models and misfits for all profiles are shown in Figures 8 and 9. Around the mine area, the rms misfit values are higher but still acceptable. The TE-TM and TE-TM-T_{zy} inversions appear to be similar except for line 276 (Figure 9). The TE-TM inversion gives a better fit to the data (Figure 8), but the model differs from the other TE-TM models. This might be because of the gap on line 276 or because the mine is located on this profile and cultural noise may have degraded the quality of the AMT data. However, this is not seen on the chosen time series data around the mine.

As noted earlier, the induction vectors for the northern profiles (lines 266-304) suggest a departure from a simple 2D geometry. Thus, tipper data from the northern profiles must be used with caution. Although the TE-TM-T_{zy} results give low rms misfits for profiles 224–254, the TE-TM inversion is more reliable for the other profiles. The rms misfits shown in Figure 8 also support this

idea because the TE-TM-T_{zy} inversions have smaller rms misfits for line 224, possibly because of the two-dimensionality indicated by the profile parallel induction vectors. The rms misfits are higher for the TE-TM-T_{zy} inversions where the induction vectors are not parallel to the profile, perhaps indicating 3D or anisotropic effects in the data.

To examine the robustness of the inversion models, a range of inversions was performed with different control parameters α and τ. The smoothing parameter τ controls the trade-off between fitting the AMT data and producing a spatially smooth model. The parameter α controls the ratio of horizontal and vertical smoothness. The resistivity models in Figure 9 were obtained with default parameters (τ = 10 and α = 1) that gave results typical of a range of α and τ values.

The conductor imaged in the inversions is located in the basement with the top at a depth of 500 m and extending to a depth of at least 2 km. In the southwestern part of the survey area, the conductor appears to dip to the southeast. Around the mine, the conductor is weaker, but the AMT data from these profiles are lower in quality than data from other profiles. In the northeastern part of the survey area, two basement conductors are imaged. The second stronger conductor could be another graphitic fault northwest of the main conductor (P2 reverse fault). The inversion results suggest that this second conductor may extend to the southwest, because the same feature can be seen just beyond the NW end of the models for profiles 224-248 (this part of the models is not shown in Figure 9). The induction vectors (Figure 6) also indicate the presence of these conductors. This is clear at 100 Hz, where induction vectors at the NW

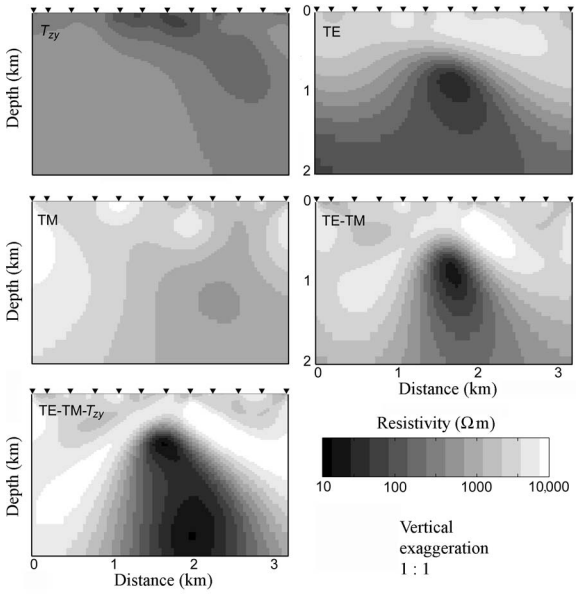

Figure 7. Resistivity models derived for profile 224 with 2D AMT inversions. The inversions for line 224 give the following root mean square (rms) misfits: T_{zy} only 1.125, TE only 2.152, TM only 0.833, TE-TM 1.703, and TE-TM-T_{zy} 1.687. An ideal misfit would be in the range of 1.0–1.5, but these values are certainly acceptable.

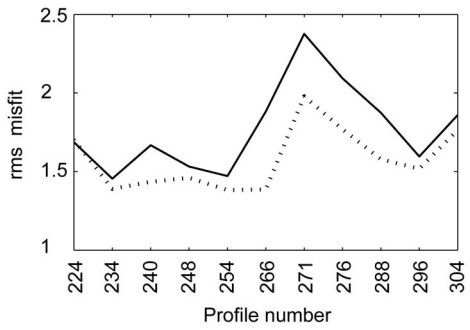

Figure 8. Root-mean-square (rms) misfit values for the TE-TM (dashed) and TE-TM-T_{zy} (solid) inversions for each profile.

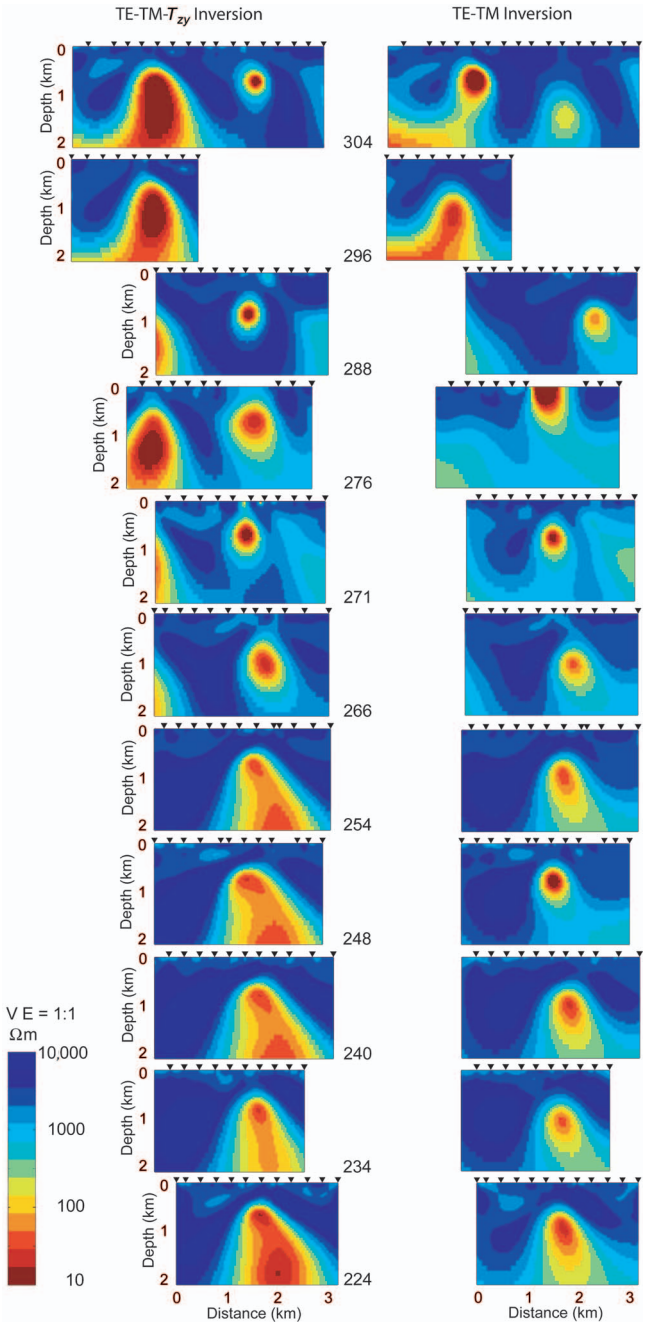

Figure 9. Resistivity models for all profiles derived with 2D inversion.

end of lines 240, 248, 254, 266, and 271 may indicate another conductor.

The other feature that is obvious in Figure 9 is a resistive halo (5000–10,000 Ω.m) that appears above and on the sides of the basement conductor. This feature is clearest on lines 224-254. This feature could be caused by the silicification or alteration associated with uranium ore formation. However, it could be an artifact of the regularization used in the inversion, because of the high resistivity contrast between the graphite conductor and the host rock.

3D inversion

The validity of the 2D inversions was investigated by performing a 3D inversion of the whole AMT data set using the algorithm of Siripunvaraporn et al. (2005a). The off-diagonal components of the impedance tensor at 16 frequencies and 131 sites were inverted using an impedance error floor of 5%. The inversion started from a 1000 Ω.m half-space and the vertical-to-horizontal smoothing ratio was set to unity. The initial and final rms misfits of the 3D inversion were 5.56 and 1.38, respectively. Figure 10 shows a comparison of the 2D and 3D inversion models with borehole log data. Note that the 3D inversion did not include the T_{zy} data. Resistivity values in the 2D and 3D models agree well in the center of the array (line 248), where both the 2D and 3D models are compatible with borehole log results. Significant differences are observed between the 2D and 3D models for line 304. These differences may be a consequence of profile 304 being on the edge of the grid of AMT data.

The 3D and 2D inversion models can also be compared as horizontal slices for different depths (Figure 11). Both inversions show that the basement conductor, the surrounding resistive halo, and all other significant model features are similar below 500 m. The conductor appears stronger in the TE-TM-T_{zy} inversion than in the other two results, probably because the T_{zy} data are primarily sensitive to the basement conductor.

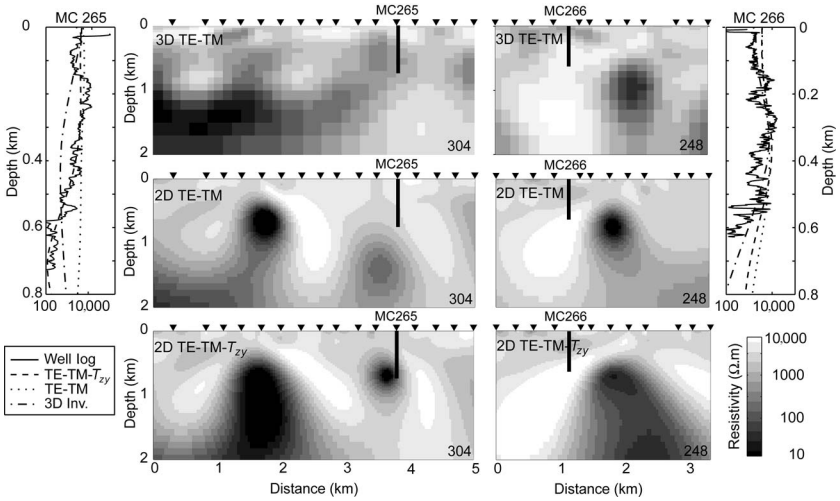

Figure 10. Comparison of 2D and 3D inversion results for lines 248 and 304. Comparison with resistivity in adjacent borehole logs is also shown.

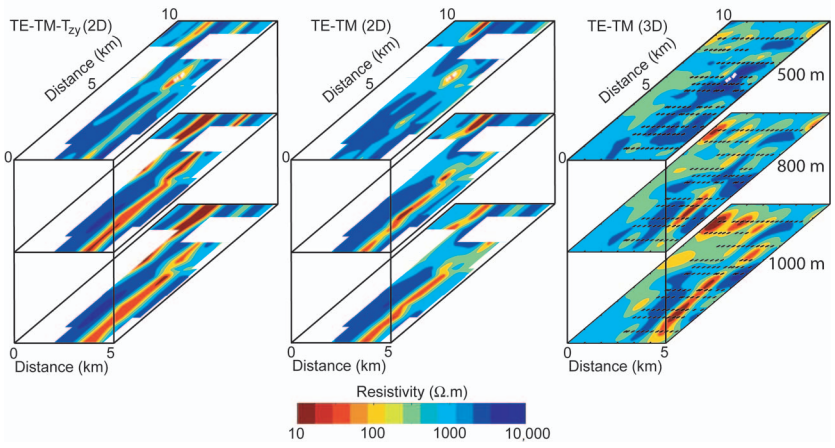

Figure 11. Comparison of the horizontal slices of the 2D and 3D inversion models. The white rectangles show the locations of the uranium pods.

VALIDATION OF INVERSION MODELS

Comparison of resistivity model with borehole logs

Extensive borehole data were acquired at the McArthur River Mine (Mwenifumbo et al., 2004). Five resistivity logs are compared with the 2D and 3D AMT inversion models in Figure 12. A 7-point moving average filter was applied to the borehole log data to allow a more objective comparison of the two measures of subsurface resistivity. The agreement between well logs and the 2D and 3D resistivity models is acceptable in the shallow wells (MC197, MC218, and RL088). However, at depths below 300 m, there are significant differences between the 2D and 3D models that may be a consequence of how deeper structure is smoothed into shallower structure. MC265 and MC266 extend deeper and terminate in a zone of lower resistivity (100 Ω.m) that is well resolved in the 2D inversion model. The 3D model agrees with the well log and 2D inversion at MC266, but agreement is poorer at MC265, perhaps because of the location of this well at the edge of the survey grid. Overall, acceptable agreement is observed between well logs and 2D inversion models. However, the basement conductor is not sampled by the well logs, and this feature dominates the spatial smoothness of the whole resistivity model. As a consequence, the different regularization used in the 2D and 3D inversion is likely the result of the differences between the 2D and 3D models.

Synthetic 2D AMT inversions

The sensitivity of the inversion models to the measured AMT data was investigated through synthetic inversions. This procedure can reveal whether features in the resistivity models are required by the AMT data or are artifacts of the inversion. Generic resistivity models were created that contain the basic resistivity features of the ore deposit. Forward modeling was then used to compute the predicted AMT data, and 5%–10% Gaussian noise was added. Then, the synthetic AMT data were inverted, using the same parameters as in the inversions of field AMT data. Many

models were considered; two representative models are shown in Figure 13. The first synthetic model represents a basement conductor, with a modest resistivity contrast across the unconformity. Figure 13 show the results of different values of α, the factor that controls the ratio of horizontal and vertical smoothness. Larger α values generate horizontal structures, and smaller values of α yield vertical structures. Because the target body in this study is a vertical, or steeply dipping, conductor, α less than one is clearly appropriate. Increasing α gives higher rms misfit values because a horizontally smooth model is incompatible with the original model. Note that the AMT inversion does not recover the correct width of the conductor. The smoothing reflects the diffusive physics of AMT exploration, and small features cannot be recovered properly. The parameter τ controls the trade-off between fitting the data and producing a spatially smooth model. Increasing τ results in a smoother model (Figure 13), and very small τ values produce a rough model with a second conductor above the basement conductor. This second conductor is clearly an artifact.

The synthetic inversion studies suggest that the values $\alpha = 1$ and $\tau = 10$ are most suitable for inversion of the field AMT data. They also show that the measured AMT data can image structures up to a depth of 2 km. Other synthetic inversions showed that the AMT data are relatively insensitive to the dip of the basement conductor. Synthetic inversions were also used to study whether the AMT data could image the structure of the alteration chimney suggested by McMullan et al. (1987). The synthetic inversion study shows that a chimney could be resolved by the AMT data. The absence of such a feature in Figure 9 suggests a low-resistivity chimney is absent at McArthur River.

Finally, synthetic inversions were used to determine if a halo of silicification could be imaged with AMT data. The model in Figure 13b includes a simple basement conductor. The synthetic inversion produces a high-resistivity halo around the basement conductor. As previously described, this is a consequence of the regularization imposed on the model during inversion. Observing a resistive halo in an inversion model does not imply that one is present in the subsurface. However, AMT data are sensitive to a resistive zone above the unconformity (Craven et al., 2003).

3D forward modeling

Three-dimensional forward modeling was used to determine if the 2D inversion results are valid in a 3D geoelectric environment. The algorithm of Mackie et al. (1994) was used and the parameterization tested by comparison with 2D modeling. The basic question to be addressed is the 3D effect of the end of the conductors on 2D inversions. A suite of models similar to that shown in Figure 14 was generated; it represents the geoelectric structure typical of the McArthur River area. An overburden layer (2000 Ωm) overlies sandstones (4000 Ωm) with 10,000 Ωm basement below the unconformity. Graphitic conductors (0.1 Ωm) are present in the basement and denoted with gray shading.

Figure 14 shows the apparent resistivity and phase curves at selected locations. The end effect is very strong on the TE mode at the north end of the conductor at site A and weaker at site B on line 224. Note that because electric charges develop on the end of the conductor in the 3D model, the TE apparent resistivity is increased at low frequency, even exceeding the TM-mode apparent resistivity. Thus, TE-mode data must be used with caution in a 3D environment (Wannamaker et al., 1984; Siripunvaraporn et al., 2005b). However, the TE mode must be used in this example because the conductor is essentially invisible to the TM-mode AMT data. However, the measured AMT data do not show the effect described above, and the TE-mode apparent resistivity is always less than the TM mode at all sta-

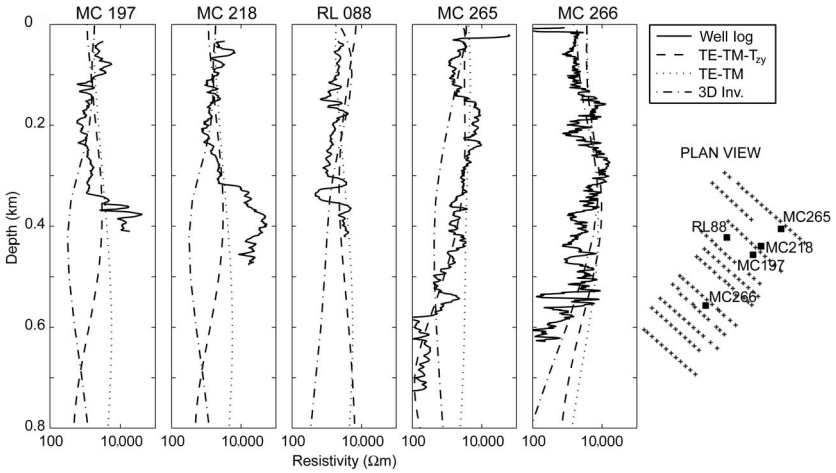

Figure 12. Comparison of borehole-log resistivity data (from Mwenifumbo et al., 2004) and inversion of 2D and 3D models.

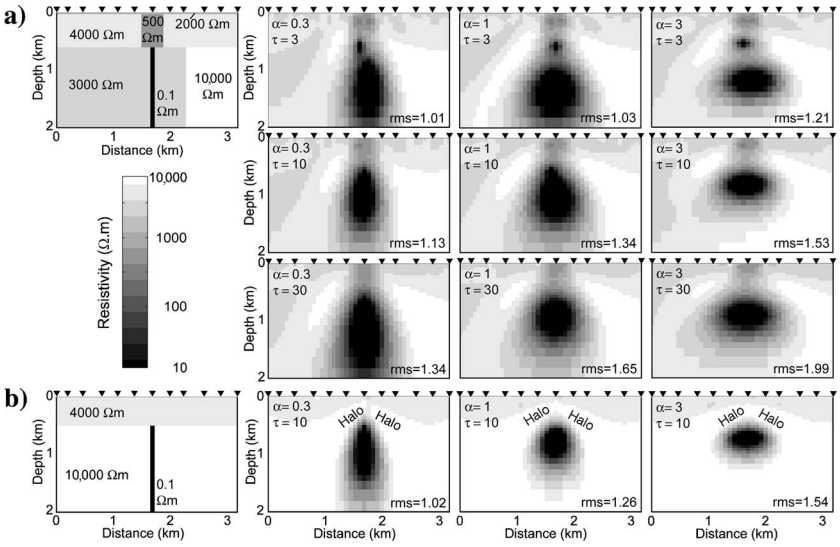

Figure 13. Synthetic inversion study showing the effect of different smoothing parameters. (a) The first model represents the alteration chimney (500 Ωm) beneath the 25-m-thick 2000-Ωm resistive overburden and shows resistivity contrast across the fault with different smoothing parameters. (b) The second model on the bottom row shows a basic two-layer model with a graphitic conductor that has an artificial resistive halo around the conductor.

tions (Figure 5). This strongly suggests that major 3D effects are not present in the field data and the McArthur River AMT data are largely two dimensional. Thus, if the basement conductor terminates close to a profile, a two dimensional inversion is not valid because the difference between the 2D and 3D forward responses is significant (Figure 14). This suggests that the resulting inversion model (Figure 15), with a graphitic conductor which terminates at the unconformity and dips to the east, is valid.

Tensor decomposition is widely used to determine if a 2D interpretation of an AMT data set is valid. Figure 3 shows the results of tensor decomposition for the synthetic data generated for the model in Figure 14. As expected, a strike direction parallel to the basement conductors is determined far from the ends, although a more complex pattern is observed close to the ends. Note that the degree of scatter in the synthetic strike directions is quite similar to that observed in the real AMT data (Figure 3). Figure 3 also shows the rms misfits, and they are significantly higher than values obtained for the field data. The rms misfit may represent a more reliable test than the strike diagrams to determine if field AMT data can be considered two dimensional.

Induction vectors were also used to assess the dimensionality of the real and synthetic AMT data. In a 2D scenario, induction vectors are orthogonal to the geoelectric strike (i.e., parallel to the profiles). Figure 6 shows that 3D effects are only observed in the induction vectors close to the ends of the conductors. The scatter of induction vectors is much less in the synthetic AMT data than in the measured AMT data. A range of other models with different geometries of basement conductors were also analyzed, and none could reproduce the observed pattern with some vectors parallel to the basement conductors. The non-2D pattern in the measured induction vectors is likely because of surficial resistivity structures outside the survey area or another conductor northeast of the survey area. Alternatively, the pattern of orthogonal induction vectors might be caused by electrical anisotropy in the basement rocks (Heise and Pous, 2001).

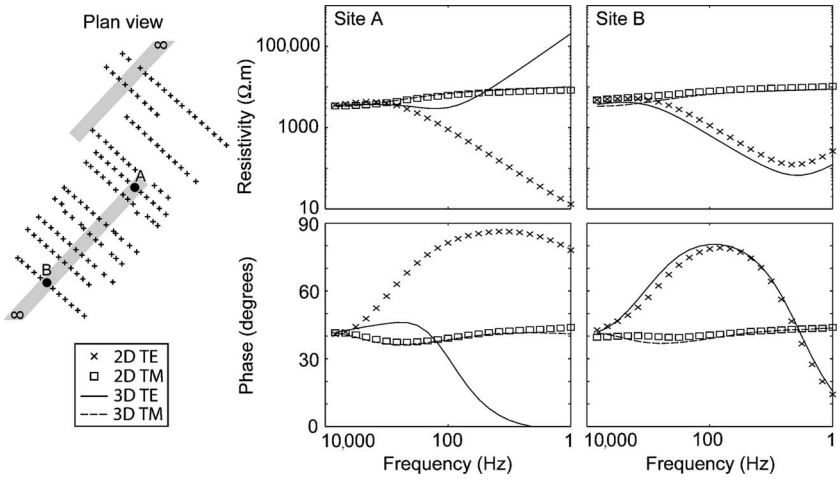

Figure 14. A 3D forward modeling study to investigate if 3D effects are present in the AMT data. Gray rectangular bars represent graphitic conductors; dark gray circles show station locations for this exercise. The apparent resistivity and phase data are shown at stations A and B for 2D and 3D resistivity models.

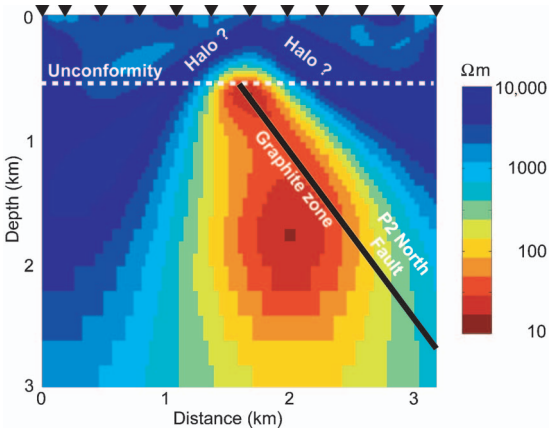

Figure 15. Interpretation of the resistivity model derived from a 2D inversion of the TE-TM-T_{zy} data for profile 224.

CONCLUSIONS

This study has shown that AMT exploration is an effective tool for mapping basement conductors to a depth of 2–3 km in a setting such as the Athabasca Basin. The P2 basement conductor imaged with AMT in this study terminates at the unconformity and may dip to the east. The resistivity model is also consistent with a zone of silicification above the orebody, but it is possible that this feature may be an artifact of the inversion algorithm. The uranium orebodies are not imaged directly because of their small size and the low-resistivity contrast between the uranium ore and graphite in the fault zone. In the type of geometry encountered in this region, the 2D inversion appears to recover subsurface resistivity with confidence, and a full 3D inversion may not always be needed. In locations where the induction vectors indicate a 2D structure, the vertical magnetic field data add useful information to the inversion and enhance its resolution. However, the vertical magnetic field data must be used with caution. Severe 3D effects can be expected in the AMT apparent-resistivity and phase data at the ends of basement conductors.

ACKNOWLEDGMENTS

AMT data collection was funded by Cameco Corporation, AREVA subsidiary COGEMA Resources Inc., the Geological Survey of Canada, and Geosystem Canada. Data analysis at the University of Alberta was supported by research grants to Martyn Unsworth from NSERC and the Alberta Ingenuity Fund. Alan Jones and Gary McNeice are thanked for the use of their tensor decomposition software. We also thank Wen Xiao, Erşan Türkoğlu, and Wolfgang Soyer for their contributions and helpful discussions. The 3D inversion at Mahidol University was supported by a research grant from the Thailand Research Fund (RSA4780021) to Weerachai Siripunvaraporn. This manuscript benefited greatly from comments by Dan Brisbin, Charlie Jefferson, and Brian Powell. Reviews by editors George Jiracek and Randy Mackie improved the paper.

REFERENCES

Berdichevsky, M. N., V. I. Dmitriev, and E. E. Pozdnjakova, 1998, On two-dimensional interpretation of magnetotelluric soundings: Geophysical Journal International, **133**, 585–606.

Chouteau, M., P. Zhang, D. J. Dion, B. Giroux, R. Morin, and S. Krivochieva, 1997, Delineating mineralization and imaging the regional structure with magnetotellurics in the region of Chibougamau (Canada): Geophysics, **62**, 730–748.

Craven, J. A., G. McNiece, B. Powell, R. Koch, I. R. Annesley, G. Wood, and C. J. Mwenifumbo, 2003, First look at data from a three-dimensional audiomagnetotelluric survey at the McArthur River mining camp, northern Saskatchewan: Geological Survey of Canada Current Research, C25, accessed August 2006 ⟨http://dsp-psd.communication.gc.ca/Collection/GSC-CGC/M44-2003/Articles/c25.pdf⟩.

Crone, J. D., 1991, PEM case histories, Cigar and Winston Lakes, Canada, *in* M. N. Nabighian ed., Electromagnetic methods in applied geophysics, vol. 2: SEG, 490–494.

Hajnal, Z., E. Takacs, D. White, B. Reilkoff, B. Powell, and R. Koch, 2002, Regional seismic images beneath the McArthur River ore bodies, Saskatchewan, *in* Summary of investigations 2002, vol. 2: Saskatchewan Geological Survey, Saskatchewan Industry Resources, Miscellaneous Report 2002–4.2, Paper D-4, accessed August 2006 ⟨http://www.ir.gov.sk.ca/adx/asp/adxGetMedia.asp?DocID=4367,3574,3442,3440,3385,2936,Documents&MediaID=8694&Filename=hajnal.pdf⟩.

Heise, W., and J. Pous, 2001, Effects of anisotropy on the two-dimensional inversion procedure: Geophysical Journal International, **147**, 610–621.

Jefferson, C. W., G. Delaney, and R. A. Olson, 2003, EXTECH IV: Athabasca uranium multidisciplinary study of northern Saskatchewan and Alberta, Part 1, Overview and impact: Geological Survey of Canada Current Research, C18, accessed August 2006 ⟨http://dsp-psd. communication. gc.ca/Collection/GSC-CGC/M44–2003/Articles/c18. pdf⟩.

Jones, A. G., and X. Garcia, 2003, Case history. Okak Bay AMT data-set case study: Lessons in dimensionality and scale: Geophysics, **68**, 70–91.

Larsen, J., R. L. Mackie, A. Manzella, A. Fiordelisi, and S. Rieven, 1996, Robust smooth magnetotelluric transfer functions: Geophysical Journal International, **124**, 801–819.

Livelybrooks, D., M. Mareschal, E. Blais, and J. T. Smith, 1996, Magnetotelluric delineation of the Trillabelle massive sulfide body in Sudbury, Ontario: Geophysics, **61**, 971–986.

Mackie, R. L., J. T. Smith, and T. R. Madden, 1994, Three-dimensional electromagnetic modeling using finite difference equations: The magnetotelluric example: Radio Science, **29**, 923–935.

McMullan, S. R., R. B. Matthews, and P. Robertshaw, 1987, Exploration geophysics for Athabasca uranium deposits: Proceedings of the Ontario Geological Survey, Exploration '87, 547–566.

McNeice, G. M., and A. G. Jones, 2001, Multisite, multifrequency tensor decomposition of magnetotelluric data: Geophysics, **66**, 158–173.

Mwenifumbo, C. J., B. E. Elliott, C. W. Jefferson, G. R. Bernius, and K. A. Pflug, 2004, Physical rock properties from the Athabasca Group: Designing geophysical exploration models for unconformity uranium deposits: Journal of Applied Geophysics, **55**, 117–135.

Parkinson, W. D., 1959, Directions of rapid geomagnetic variations: Geophysical Journal of the Royal Astronomical Society, **2**, 1–14.

Rodi, W., and R. Mackie, 2001, Nonlinear conjugate gradients algorithm for 2D magnetotelluric inversion: Geophysics, **66**, 174–187.

Ruzicka, V., 1996, Unconformity associated uranium: Geology of Canada, **8**, 197–210.

Siripunvaraporn, W., G. Egbert, Y. Lenbury, and M. Uyeshima, 2005a, Three-dimensional magnetotelluric inversion: Data-space method: Physics of the Earth and Planetary Interiors, **150**, 3–14.

Siripunvaraporn, W., G. Egbert, and M. Uyeshima, 2005b, Interpretation of two-dimensional magnetotelluric profile data with three-dimensional inversion: Synthetic examples: Geophysical Journal International, **160**, 804–814.

Wannamaker, P. E., G. W. Hohmann, and S. H. Ward, 1984, Magnetotelluric responses of three-dimensional bodies in layered earths: Geophysics, **49**, 1517–1533.

White, D. J., Z. Hajnal, I. Gyorfi, E. Takacs, B. Roberts, C. Mueller, B. Reilkoff, R. Koch, B. Powell, I. R. Annesley, S. Bernier, and C. W. Jefferson, 2003, Interim results of the EXTECH-IV seismic-reflection program in the Athabasca Basin, northern Saskatchewan: Geological Survey of Canada Current Research, C8, accessed August 2006 ⟨http://dsp-psd.communication.gc.ca/Collection/GSC-CGC/M44-2003/Articles/c08.pdf⟩.

White, D. J., B. Roberts, C. Mueller, Z. Hajnal, I. Gyorfi, B. Reilkoff, R. Koch, and B. Powell, 2002, Seismic reflection profiling: An effective exploration tool in the Athabasca Basin? An interim assessment, *in* Summary of investigations 2002, Vol. 2, Saskatchewan Geological Survey, Saskatchewan Industry Resources, Miscellaneous Report 2002–4.2, Paper D-2, accessed August 2006 ⟨http://www.ir.gov.sk.ca/adx/asp/adxGetMedia.asp?DocID=4367,3574,3442,3440,3385,2936,Documents&MediaID=8692&Filename=white. pdf⟩.

Wood, G., and M. D. Thomas, 2002, Modeling of high-resolution gravity data near the McArthur River uranium deposit, Athabasca Basin: Summary of Investigations 2002, Vol. 2, Saskatchewan Geological Survey, Saskatchewan Industry Resources, Miscellaneous Report 2002–4.2, PaperD-16, accessed August 2006 ⟨http://www.ir.gov.sk.ca/adx/asp/adxGetMedia.asp?DocID=4367,3574,3442,3440,3385,2936,Documents&MediaID=8706&Filename=wood. pdf⟩.